A Journal of the Gesellschaft Deutscher Chemiker

Angewandte International Edition GDCh Chemie

www.angewandte.org

Accepted Article

Title: Alkynyl-Protected Chiral Bimetallic Ag22Cu7 Superatom with Multiple Chirality Origins

Authors: Guocheng Deng, Kangjae Lee, Hongwen Deng, Sami Malola, Megalamane S. Bootharaju, Hannu Häkkinen, Nanfeng Zheng, and Taeghwan Hyeon

To be cited as: *Angew. Chem. Int. Ed.* **2022**, e202217483

Link to VoR: https://doi.org/10.1002/anie.202217483

WILEY-VCH

10.1002/anie.202217483

RESEARCH ARTICLE

WILEY-VCH

Alkynyl-Protected Chiral Bimetallic $Ag_{22}Cu_7$ Superatom with Multiple Chirality Origins

Guocheng Deng[+], Kangjae Lee[+], Hongwen Deng[+], Sami Malola, Megalamane S. Bootharaju,* Hannu Häkkinen,* Nanfeng Zheng* and Taeghwan Hyeon*

[*] Dr. G. C. Deng, K. Lee, Dr. M. S. Bootharaju, Prof. T. Hyeon
Center for Nanoparticle Research, Institute for Basic Science (IBS), School of Chemical and Biological Engineering, and Institute of Chemical Processes, Seoul National University
Seoul 08826, Republic of Korea
E-mail: thyeon@snu.ac.kr, msbootharaju@snu.ac.kr

H. W. Deng, Prof. N. F. Zheng
Collaborative Innovation Center of Chemistry for Energy Materials, State Key Laboratory for Physical Chemistry of Solid Surfaces, and National & Local Joint Engineering Research Center of Preparation Technology of Nanomaterials, College of Chemistry and Chemical Engineering, Xiamen University
Xiamen 361005, China
E-mail: nfzheng@xmu.edu.cn

Dr. S. Malola, Prof. H. Häkkinen
Departments of Physics and Chemistry, Nanoscience Center, University of Jyväskylä
FI-40014 Jyväskylä, Finland
E-mail: hannu.j.hakkinen@jyu.fi

[+] These authors contributed equally to this work.

Supporting information for this article is given via a link at the end of the document.

Abstract: Understanding the origin of chirality in the nanostructured materials is essential for chiroptical and catalytic applications. Here we report a chiral AgCu superatomic cluster, $[Ag_{22}Cu_7(C{\equiv}CR)_{16}(PPh_3)_5Cl_6](PPh_4)$, **$Ag_{22}Cu_7$**, protected by an achiral alkynyl ligand (HC≡CR: 3,5-bis(trifluoromethyl)phenylacetylene). Its crystal structure comprises a rare interpenetrating biicosahedral $Ag_{17}Cu_2$ core, which is stabilized by four different types of motifs: one $Cu(C{\equiv}CR)_2$, four -C≡CR, two chlorides and one helical $Ag_5Cu_4(C{\equiv}CR)_{10}(PPh_3)_5Cl_4$. Structural analysis reveals that **$Ag_{22}Cu_7$** exhibits multiple chirality origins, including the metal core, the metal-ligand interface and the ligand layer. Furthermore, the circular dichroism spectra of **R/S-$Ag_{22}Cu_7$** are obtained by employing appropriate chiral molecules as optical enrichment agents. DFT calculations show that **$Ag_{22}Cu_7$** is an eight-electron superatom, confirm that the cluster is chirally active, and help to analyze the origins of the circular dichroism.

Introduction

Monolayer-protected superatomic alloy nanoclusters of coinage metals have attracted substantial research attention in the past decade mainly due to their improved physicochemical properties as compared to the corresponding monometallic counterparts.[1] Alkynyl molecules, as a new type of protecting ligands for the nanoclusters, have garnered a great deal of interest owing to their diverse coordination modes with the metals *via* both π and σ bonding,[2] unlike the widely studied thiolate ligands, which exhibit either terminal or bridging binding modes.[3] Extended metal-carbon interactions endow alkynyl-protected nanoclusters with numerous types of surface motifs, which enabled the realization of nanoclusters with novel structures and optical and catalytic properties.[2, 4] Similar atomic radii and complete miscibility of Ag and Au in one another in the bulk phase have resulted in the chemical synthesis and structural characterization of several alkynyl-protected bimetallic AuAg nanoclusters.[5] In contrast, the alkynyl-protected Cu-containing nanoclusters are rarely achieved due to synthetic challenges, which in turn due to their instability. So far, only one alkynyl-protected AuCu alloy superatomic nanocluster $[Au_{19}Cu_{30}(C{\equiv}CAr)_{22}(Ph_3P)_6Cl_2](NO_3)_3$ is reported to date (HC≡CAr: 3-ethynylthiophene or ethynylbenzene),[6] indicating more room to unearth the alloy nanoclusters of novel size, structure and properties by employing alkynyl ligands. However, for the combination of Ag and Cu, the alkynyl ligands have been used to obtain M(I) clusters (M: Ag/Cu) such as Ag_3Cu_5,[7] Ag_8Cu_6,[4d, 8] $Ag_{16}Cu_9$,[9] and $Ag_{25}Cu_4H_8$.[10] Only recently, Tang *et al.*, described the synthesis of the $[Ag_9Cu_6(^tBuC{\equiv}C)_{12}]^+$ cluster containing two free valence electrons.[11] However, high-nuclearity alkynyl-protected AgCu superatoms with a large number of free electrons and a richer structural diversity yet to be reported.

Furthermore, the chiral metal nanoclusters are ideal model platforms to probe into the atomic-level origins of chirality of metal nanoparticles.[12] In recent years, several chiral metal nanoclusters with the atomic-level structures have been reported.[13] The chirality of metal nanoclusters is anticipated to originate from the following three possibilities: asymmetric atomic arragements in the metal core, metal-ligand interface and ligand layer.[12b] Due to the inherent achiral nature of bulk metals, the synthesis of metal-based nanomaterials with chiral metal cores had been considered to be not trivial, let alone metal-based nanomaterials with multiple-level chirality origins such as above mentioned scenarios. Therefore, it is of great significance to explore the existing nanocluster families to achieve clusters with novel structures and rich chiral characteristics.

Herein, we report the synthesis and total structure of an alkynyl-protected chiral bimetallic AgCu superatomic nanocluster, $[Ag_{22}Cu_7(C{\equiv}CR)_{16}(PPh_3)_5Cl_6](PPh_4)$ (abbreviated hereafter as **$Ag_{22}Cu_7$**), which comprises eight free valence electrons. The composition, atomic-level structure and electronic structure of

$Ag_{22}Cu_7$ are thoroughly characterized by various experimental and computational methods, including electrospray ionization mass spectrometry (ESI-MS), single-crystal X-ray diffraction (SCXRD), elemental analysis, optical spectroscopy and density functional theory (DFT) calculations. The multiple-level chirality of **$Ag_{22}Cu_7$**, originating from the metal core, the metal-ligand interface, and the phenyl groups of alkynyl ligands, is revealed through a detailed structural analysis. Furthermore, by using appropriate chiral molecules as optical enrichment agents, such as R/S-(3,5-dioxa-4-phosphacyclohepta[2,1-a;3,4-a']dinaphthalen-4-yl)dimethylamine), the **$Ag_{22}Cu_7$** is converted into corresponding enantiomers and their circular dichroism spectra are recorded. DFT calculations confirm that the cluster is optically active, and help to analyze the origins of the circular dichroism. This work paves the way to the synthesis of high-nuclearity alkynyl-protected AgCu alloy superatoms with novel structures and properties.

Results and Discussion

The **$Ag_{22}Cu_7$** nanocluster is synthesized by designing a facile one-pot route involving the reaction of AgC≡CR complexes with $(PPh_3)_2CuBH_4$ in the presence of PPh_4Cl in a mixed solvent system of CH_2Cl_2/MeOH at room temperature (see Supporting Information, SI, for more details). Rod-like black crystals are grown by the diffusion of *n*-hexane into a CH_2Cl_2 solution of **$Ag_{22}Cu_7$** at a low temperature of -12 ºC (Figure S1). It is worth mentioning that the low temperature is crucial in obtaining the good-quality single crystals of **$Ag_{22}Cu_7$**.

The chemical composition and charge-state of **$Ag_{22}Cu_7$** are determined by the ESI-MS. As shown in Figure S2, a prominent peak is apparent at m/z: 8136, which corresponds to the molecular ion $[Ag_{22}Cu_7(C{\equiv}CR)_{16}(PPh_3)_5Cl_6]^-$ (calculated m/z: 8136.08). Furthermore, the experimental isotopic distribution pattern is in good agreement with the simulated isotopic pattern (Figure S2, inset). The transmission electron microscopy (TEM) and high-angle annular dark field-scanning transmission electron microscopy (HAADF-STEM) analyses showed that **$Ag_{22}Cu_7$** cluster is highly monodispersed with a diameter of ~1.4 nm (Figure S3), which matches well with that (1.3 nm) obtained from the X-ray crystallographic data (see below). The scanning electron microscopy energy dispersive X-ray spectroscopy (SEM EDS) analysis showed the presence of Ag, Cu, P and Cl elements in **$Ag_{22}Cu_7$** (Figure S4). Consistently, the X-ray photoelectron spectroscopy (XPS) analysis (Figure S5) confirmed the elements (Ag, Cu, P, Cl, F and C) of **$Ag_{22}Cu_7$**. The Ag $3d_{5/2}$ peak at 368.0 eV indicates the valence state of Ag to be between Ag(0) and Ag(I).[15]

The atomic-level structure of **$Ag_{22}Cu_7$** is determined by the analysis of SCXRD data. This nanocluster crystallizes in the centrosymmetric space group *Pbca* (No. 61) (Table S1). Figure S6 shows the packing of the **$Ag_{22}Cu_7$** clusters in the crystal lattice, wherein the unit cell comprises four pairs (Z=8) of enantiomers of clusters. The overall structure of **$Ag_{22}Cu_7$** is shown in Figure 1, revealing the presence of 22 silver atoms, 7 copper atoms, 16 -C≡CR ligands, 5 triphenylphosphine ligands and 6 chlorides. This composition, $Ag_{22}Cu_7(C{\equiv}CR)_{16}(PPh_3)_5Cl_6$, is consistent with the ESI-MS data (Figure S2). A counter-cation (PPh_4^+) is located in the crystal structure, indicating that the **$Ag_{22}Cu_7$** is a mono anionic eight-electron superatom (Table S1).

The structure of **$Ag_{22}Cu_7$** can be visualized as the capping of the $Ag_{17}Cu_2$ metal core with a metal-ligand shell of $Ag_5Cu_5(C{\equiv}CR)_{16}(PPh_3)_5Cl_6$.

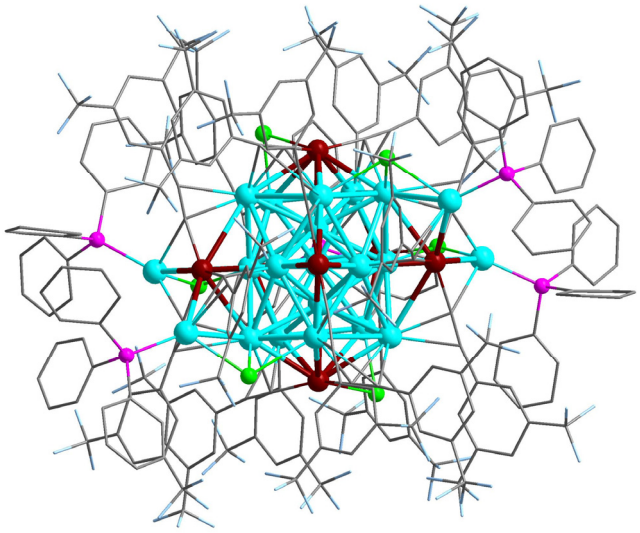

Figure 1. Molecular structure of **$Ag_{22}Cu_7$**. Color legend: turquiose, Ag; dark red, Cu; bright green, Cl; pink, P; pale blue, F; grey, C. All hydrogen atoms are omitted for clarity.[14]

The anatomy of the structure of **$Ag_{22}Cu_7$** is illustrated in Figure 2. Analysis of the $Ag_{17}Cu_2$ core shows an Ag_2 inner core surrounded by $Ag_{15}Cu_2$ in the form of $Ag_2@Ag_{15}Cu_2$. The formation of $Ag_{17}Cu_2$ core (Figure 2a) can be described as the interpenetration of two $Ag_{11}Cu_1$ hollow icosahedra followed by sharing of an Ag_5 plane. Notably, the Cu atoms are found to occupy preferentially the top and bottom vertices of $Ag_{17}Cu_2$, imparting a prolate shape to the core with an atomic arrangement of 1Cu:5Ag:1Ag:5Ag:1Ag:5Ag:1Cu (Figure S7). The Ag atoms in the $Ag_{17}Cu_2$ core have an average Ag-Ag bond length of 2.915 Å, slightly longer than the Ag-Ag distance (2.889 Å) in the bulk face-centered cubic (fcc) silver. However, the bond length of the two inner Ag atoms is found to be 2.664 Å, which is much shorter than the Ag-Ag distance in the bulk silver, indicating the strong interaction between the two interpenetrating icosahedra.

Two Cl atoms cap two Ag-Cu bonds, formed between the vertex Cu atoms and nearby Ag atoms of the two Ag_5 planes of the $Ag_{17}Cu_2$ core, in μ_2 mode (Figure 2b) such that these two Cl atoms are opposite to each other. One Cu atom is coordinated with one of the edges of the middle Ag_5 plane (i.e., the shared Ag_5 plane). Then, each Cu atom is coordinated with two alkynyl ligands to form the structure of $Ag_{17}Cu_3Cl_2(C{\equiv}CR)_6$ (Figure 2b). Finally, the protection of $Ag_{17}Cu_3Cl_2(C{\equiv}CR)_6$ structure with a metal-ligand shell of $Ag_5Cu_4(C{\equiv}CR)_{10}(PPh_3)_5Cl_4$ forms the total structure of **$Ag_{22}Cu_7$**. As shown in Figures 2c and S8a, each of the five Ag atoms of the $Ag_5Cu_4(C{\equiv}CR)_{10}(PPh_3)_5Cl_4$ metal-ligand shell is ligated by a PPh_3 molecule. The shell can be further divided into three parts, two $(AgPPh_3)_2(CuC{\equiv}CR)_3Cl_2$ units with Cl-Ag-Cu-Ag-Cl arrangement (in an "M" shape) (Figure S8b, c) and one $(AgPPh_3)_1(CuC{\equiv}CR)_2$ unit with Cu-Ag-Cu arrangement (in a "V" shape) (Figure S8d). These three parts are connected through Cu-Cl bonds with the presence of two "M" shape units on two sides of the "V" shape unit (Figure S8).

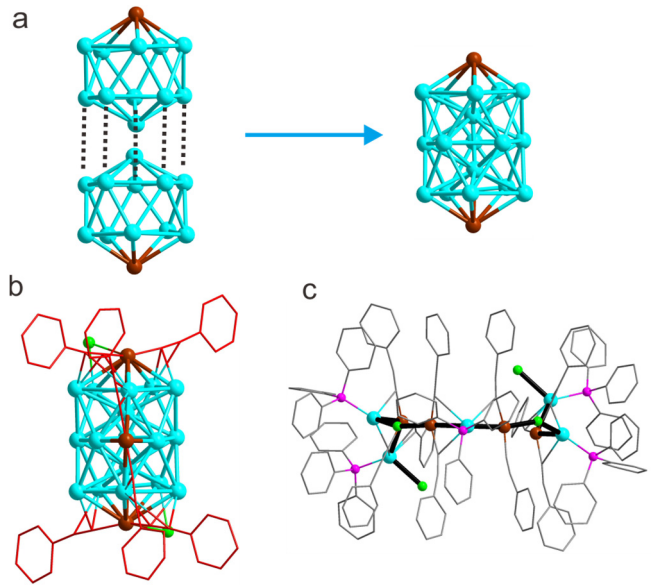

Figure 2. Structural analysis of **$Ag_{22}Cu_7$**. a) Formation of an interpenetrating biicosahedral $Ag_{17}Cu_2$ metal core through sharing of an Ag_5 plane. b) Structure of $Ag_{17}Cu_3Cl_2(C{\equiv}CR)_6$. c) Side view of the $Ag_5Cu_4(C{\equiv}CR)_{10}(PPh_3)_5Cl_4$ metal-ligand shell. Color legend: turquiose, Ag; dark red, Cu; bright green, Cl; pink, P; red or grey, C. Hydrogen atoms and trifluoromethyl groups are omitted for clarity.

Two Cl atoms cap two Ag-Cu bonds, formed between the vertex Cu atoms and nearby Ag atoms of the two Ag_5 planes of the $Ag_{17}Cu_2$ core, in μ_2 mode (Figure 2b) such that these two Cl atoms are opposite to each other. One Cu atom is coordinated with one of the edges of the middle Ag_5 plane (i.e., the shared Ag_5 plane). Then, each Cu atom is coordinated with two alkynyl ligands to form the structure of $Ag_{17}Cu_3Cl_2(C{\equiv}CR)_6$ (Figure 2b). Finally, the protection of $Ag_{17}Cu_3Cl_2(C{\equiv}CR)_6$ structure with a metal-ligand shell of $Ag_5Cu_4(C{\equiv}CR)_{10}(PPh_3)_5Cl_4$ forms the total structure of **$Ag_{22}Cu_7$**. As shown in Figures 2c and S8a, each of the five Ag atoms of the $Ag_5Cu_4(C{\equiv}CR)_{10}(PPh_3)_5Cl_4$ metal-ligand shell is ligated by a PPh_3 molecule. The shell can be further divided into three parts, two $(AgPPh_3)_2(CuC{\equiv}CR)_3Cl_2$ units with Cl-Ag-Cu-Ag-Cl arrangement (in an "M" shape) (Figure S8b, c) and one $(AgPPh_3)_1(CuC{\equiv}CR)_2$ unit with Cu-Ag-Cu arrangement (in a "V" shape) (Figure S8d). These three parts are connected through Cu-Cl bonds with the presence of two "M" shape units on two sides of the "V" shape unit (Figure S8).

Interestingly, the coordination modes of alkynyl ligands on the surface of **$Ag_{22}Cu_7$** are quite diverse. A total of three alkynyl ligands appear in μ_2 mode, connecting one Ag atom and one Cu atom as shown in Figure S9a; 11 alkynyl ligands are found to exhibit μ_3-type bridges on Ag_2Cu_1 planes (Figure S9b); and finally, two alkynyl ligands are found to enter Ag_3Cu_1 tetrahedra and bind *via* μ_4 mode (Figure S9c). The first two coordination modes (μ_2 and μ_3) are commonly observed in alkynyl-protected Au, Ag, or bimetallic AuAg, AuCu clusters.[5b, 5c, 6, 16] However, μ_4-type coordination of alkynyl ligands with metals is rare. All the 16 alkynyl ligands in **$Ag_{22}Cu_7$** coordinate with Cu atoms *via* σ-type bonding and with silver atoms *via* π-type bonding. The Cu-C and Ag-C bond lengths fall in the range of 1.787-2.063 and 2.257-2.673 Å, respectively.

Nanoclusters with atomically precise structures are potential platforms to unveil the origin of chirality at the atomic-level. In order to reveal the origin of chirality in **$Ag_{22}Cu_7$**, we carried out a detailed structural analysis of its core ($Ag_{17}Cu_2$), metal-ligand interface ($Ag_5Cu_4Cl_4$ helix) and ligand layer (phenyl groups of alkynyl ligands). It is well-known that the ideal M_{12} icosahedron has I_h symmetry and it is achiral. All the M-M bond lengths are identical and all the dihedral angles between the planes of the M atoms from the M_5 rings and two axial M atoms are 36º (Figure S10). In the case of **$Ag_{22}Cu_7$**, the $Ag_{17}Cu_2$ core contains three Ag_5 rings, upper (turquiose), middle (red) and lower (blue) as shown in Figure S11. The Ag-Ag bond lengths within the Ag_5 rings and the Ag-Cu bond lengths between Cu atoms and upper (or lower) Ag_5 rings are different, and their ranges are 2.902-3.402 and 2.867-3.519 Å, respectively (Figure S11). This observation implies that the interpenetrating biicosahedral core is distorted (Figure 3a). Furthermore, the dihedral angles between the planes formed by the Ag atoms from the upper and middle (or the middle and lower) Ag_5 rings and two axial Cu atoms are far from the ideal angle 36º (Figures 3b and S12) and vary from 28.3º to 46.2º. This reduces the symmetry of the $Ag_{17}Cu_2$ core to C_1 and therefore it is chiral.

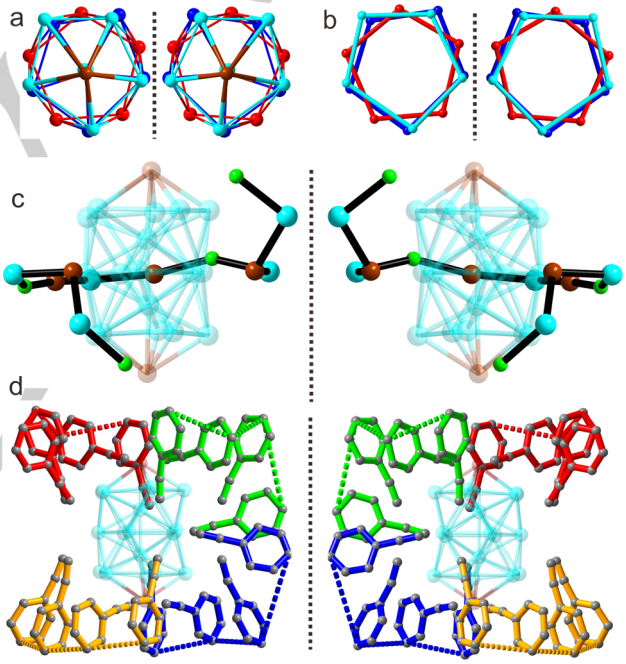

Figure 3. a) Top view of the chiral $Ag_{17}Cu_2$ core. b) Top view of the three Ag_5 rings in $Ag_{17}Cu_2$ core. c) The $Ag_5Cu_4Cl_4$ helical stripe surrounds the metal core. d) Asymmetric arrangement of the surface alkynyl ligands. Color legend: turquoise, red or blue, Ag; dark red, Cu; bright green, Cl; grey, C.

Next, the metal-ligand interface of **$Ag_{22}Cu_7$** is analyzed. Between the prolate-shaped $Ag_{17}Cu_2$ core and the surface phenyl groups of the ligands, there exists a “stripe“ consisting five Ag, four Cu and four Cl atoms ($Ag_5Cu_4Cl_4$). As shown in Figure 3c, the stripe has a helical structure with Cl-Ag-Cu-Ag-Cl-Cu-Ag-Cu-Cl-Ag-Cu-Ag-Cl arrangement. It surrounds the metal core and rotates clockwise or counterclockwise in the different enantiomers, which gives rise to chirality in **$Ag_{22}Cu_7$**.

Finally, the arrangement of surface ligands of **$Ag_{22}Cu_7$** is also investigated carefully. The 16 alkynyl ligands can be divided into four groups and each group comprises four alkynyls (Figure 3d). Two groups of them are assembled on the upper part of the

prolate-shaped $Ag_{17}Cu_2$ core and two groups on the lower part. Interestingly, all four groups of alkynyl ligands are randomly assembled on the core. No inversion centers or mirror planes exist, and thus it is an asymmetric arrangement (Figure 3d). The above analysis clearly shows that the metal core, the metal-ligand interface, and the ligand-shell of **$Ag_{22}Cu_7$** are chiral, exhibiting chirality through multiple origins.

Further characterization of the synthesized cluster was done computationally using DFT with software called GPAW.[17] The experimental structure of **$Ag_{22}Cu_7$** was optimized with PBE functional after which the electronic properties were calculated with GLLB-SC functional (for details, see the SI). Structural optimization with PBE leads to overall expansion of the system by 2-3% which is typical for these systems and is caused by the overestimation of metal-metal bond distances. Most importantly, the relative distortion of the metal core bonds shown in the Figures S13 and S14 are maintained under optimization and the structure does not get symmetrized.

Projected density of states shown in Figure 4 confirms the superatomic nature of the cluster fitting to 8e system. The highest occupied states obey P-symmetry as the lowest unoccupied states are D-symmetric which are delocalized at the metal core due to the free valence electrons. The superatom states are clearly separated from the other states including ligands and metal-ligand interface. Splitting of the superatom states can be explained by the distortion from the perfectly spherical system that is the underlying reference as using spherical harmonics functions in the projection. HOMO-LUMO gap of the system is 1.18 eV. Bader charges shown in Table S2 confirm the electron withdrawing nature of alkynes and chlorine being clearly negatively charged –0.434 |e| and –0.617 |e|. Cu-atoms are on average 1.5 times more positively charged +0.373 |e| compared to Ag-atoms in the center +0.226 |e| or at the metal core surface +0.275 |e|.

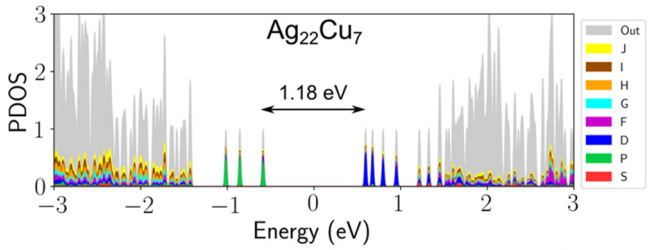

Figure 4. Electronic density of states of **$Ag_{22}Cu_7$** projected to spherical harmonics functions centered at the center of the mass of the cluster. Different colors denote projection weights at different angular momenta. The HOMO-LUMO gap is centered at E=0.

Optical absorption spectrum was calculated with linear response time-dependent density functional theory (lr-TDDFT). As shown in Figure 5a, the measured UV/Vis spectrum of the **$Ag_{22}Cu_7$** solution exhibits two strong peaks at 430 and 496 nm, and three shoulder peaks at 575, 637 and 800 nm. The UV/Vis spectrum of the single crystals of **$Ag_{22}Cu_7$** is found to be very similar to that of the **$Ag_{22}Cu_7$** solution in terms of both absorption profile and peak positions (Figure S15). This observation suggests that the size of the cluster (i.e., **$Ag_{22}Cu_7$**) determined from the SCXRD is retained in the solution, which is also consistent with the intact size of the cluster in the ESI-MS analysis of the **$Ag_{22}Cu_7$** solution (Figure S2). Furthermore, the overall agreement between the experimental and calculated spectrum (Figure 5b) is very good. In both spectra, there are four distinguishable features A-D. As a minor contradiction, there are two low intensity maxima constructing the feature labeled with B in the experimental spectrum but calculations describe the same feature with one broad peak. Optical gap is found at 1000 and ~900 nm in calculated and experimental data, respectively. The redshift in the low-energy region of the calculated spectrum is relatively small, approximately 0.14 eV. The origins of the spectral features were analyzed using the so called dipole transition contribution map (DTCM), which shows the strengthening and screening contributions to the total transition dipole moment as decomposed to Kohn-Sham electron-hole basis. The DTCM plot in Figure S13 shows that the lowest energy peaks A-C are due to different combinations of P to D superatom state transitions. The highest energy peak has main contribution from transitions between the P-states and the unoccupied ligand states localized mainly on alkynyls as shown in Figure S14 describing the localization of the states to different atoms. It is interesting to notice that the localization to the alkynyls and phosphines is seen at totally different energies in the occupied and unoccupied states. Alkynyl states are seen below -3.0 eV, between –2.5 eV and –1.5 eV, and between 1.5 eV and 2.0 eV, whereas phosphine states are seen between –3.0 eV and –2.5 eV, and between 2.0 eV and 3.0 eV. This opens intriguing questions about the possible sources and strength of chirality.

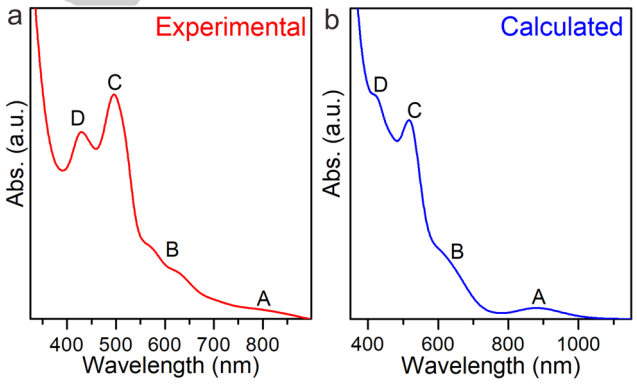

Figure 5. a) Experimental and b) calculated UV/Vis spectra of **$Ag_{22}Cu_7$**. Calculated spectrum has been broadened with Gaussian functions with 0.1 eV broadening.

The solution-state stability of **$Ag_{22}Cu_7$** is found to be moderate (Figure S16) under ambient conditions (air, 25 °C), which restricted us from the separation of enantiomers using chiral high-pressure liquid chromatography. This behavior reminds us of the poor stability of the racemic $[Ag_{28}Cu_{12}(SR)_{24}]^{4-}$ cluster solution (SR: 2,4-dichlorobenzenethiolate).[18] The chiral counter-cations are employed as chiral resolution agents to obtain the corresponding enantiomeric clusters.[18] Unfortunately, the chiral counterion strategy could not resolve the enantiomers of **$Ag_{22}Cu_7$**, which may be due to the low charge of the cluster (i.e., only 1^-). Recently, Zang and coworkers used small chiral molecules, such as R-/S-propylene oxide, in achieving pronounced CD response through inducing structural distortion in racemic R-/S-Ag_{13}@$Ag_{16}Cu_4$ clusters.[19] Inspired by this

report, here a pair of chiral monoamine molecules, R/S-(3,5-dioxa-4-phosphacyclohepta[2,1-a;3,4-a']dinaphthalen-4-yl)dimethylamine (**R/S-MA**, Figure S17), are employed to obtain the CD spectra of **R/S-$Ag_{22}Cu_7$.**

The CD spectra of the cluster solutions to which **R-** or **S-MA** is added (denoted as **R-** or **S-$Ag_{22}Cu_7$**, respectively) show characteristic features at 580, 532, 502, 563, 412 and 367 nm (A-F, respectively in Figure 6a) with perfect mirror images in the 350-700 nm region. These six features indeed belong to **$Ag_{22}Cu_7$** since pure **R-** and **S-MA** show CD peaks at 331, 317 and 306 nm, which are well below 350 nm (Figure S18). After the addition of **R-MA** to the **$Ag_{22}Cu_7$**, the characteristic absorption peaks of **$Ag_{22}Cu_7$** are retained without the appearance of new peaks (Figure S19). The ^{31}P nuclear magnetic resonance (NMR) spectra of **$Ag_{22}Cu_7$** before and after adding **R-MA** are very similar (Figure S20), indicating that the PPh_3 ligands of the clusters are not substituted by the chiral molecules. In addition, ESI-MS data show unchanged size of the cluster (Figure S21). The retained absorption features and the cluster size together demonstrate the intact structure of the cluster after adding **R-MA**. The intensities of CD peaks diminish slowly over time (Figure S22), which is due to the instability of the clusters in solution as evidenced by the weakening of the UV/Vis peaks over time (Figure S19). This rules out the possibility that one enantiomer of the cluster is stabilized by chiral molecules, while the other enantiomer is decomposed. Notably, the CD peaks appear immediately (within one minute) after the addition of **R-MA** to **$Ag_{22}Cu_7$** (Figure S22), and the intensities of the absorption spectra before and after adding **R-MA** did not change significantly within the same time window (Figure S19), indicating that the clusters are converted into the corresponding enantiomer (**R-$Ag_{22}Cu_7$**). Interestingly, the **$Ag_{22}Cu_7$** solution containing **R-MA** shows a substantially low-decrease of the absorption peak intensities (Figure S19) as compared to that without **R-MA** (Figure S16), suggesting that the chiral molecules induce not only the enrichment of the corresponding enantiomer, but also stabilize the cluster through interactions. Due to the bulkiness and associated large steric hindrance of **R-MA**, the exchange of PPh_3 of the cluster with **R-MA** seems to be prevented. Since the addition of **R-MA** did not change the size of the **$Ag_{22}Cu_7$** cluster (Figures S19-S21), the non-covalent interactions, such as C-H...F, C-H...π and π...π, are anticipated to drive the enantiomer and optical enrichment.

Although multiple chirality origins are unambiguously elucidated for the single crystals of **$Ag_{22}Cu_7$** (Figure 3), the origin of CD signals of **$Ag_{22}Cu_7$** solution after the addition of **R-** or **S-MA** needs to be discussed. Note that the chirality of the cluster origniates either from intrinsic asymmetry within the cluster or asymmetric packing effects in the crystalline state. In the former case, after dissolving the single crystals of **$Ag_{22}Cu_7$** in the solvent (toluene), intrinsic chirality of **$Ag_{22}Cu_7$** retains and the sample exists as a racemic mixture. When **R-** or **S-MA** is added to this solution, the racemic **$Ag_{22}Cu_7$** converges to corresponding enantiomers, generating CD signal. In the latter case, the chirality present in the crystalline state disappears when the cluster is dissolved in the solvent (toluene) due to transformation from racemic to achiral **$Ag_{22}Cu_7$**. Now, the chirality of **R-** or **S-$Ag_{22}Cu_7$** is generated after the interaction of achiral **$Ag_{22}Cu_7$** with **R-** or **S-MA**. The experimental verification of these possibilities in solution is highly challenging, and it requires exhaustive *in situ* chiral chromatographic and CD studies. Since the interconversion of enantiomers of chiral clusters is possible in solution,[20] the stabilized interactions (Figure S19) between clusters (racemic or achiral **$Ag_{22}Cu_7$**) and chiral molecules (**R-** or **S-MA**) would accelerate the conversion of the dissolved **$Ag_{22}Cu_7$** clusters into corresponding enantiomer, leading to optical enrichment. The high reactivity of the clusters in solution, which inturn due to the moderate solution-state stability of **$Ag_{22}Cu_7$** (Figure S16), would also contribute to steer the rapid conversion with the addition of chiral molecules.

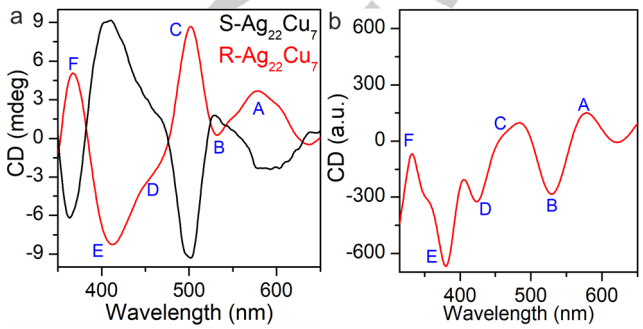

Figure 6. a) Experimental CD spectra of **R/S-$Ag_{22}Cu_7$**. b) Calculated CD spectrum of **R-$Ag_{22}Cu_7$**. Calculated spectrum has been broadened with Gaussian functions with 0.1 eV broadening.

The chirality of **$Ag_{22}Cu_7$** is investigated through DFT as well. As hypothesized in the previous sections, the structural details and electronic structure permit plausible chirality interpretations in various levels. The calculated CD spectrum is shown in Figure 6b, whcih is in good agreement with the experimental data with CD features A-F. It can be realized that the overall CD-intensities are not the strongest among similar sized clusters, for example $Au_{38}(PET)_{24}$ produces 4-5 times higher peak intensities.[21] The overall behavior of the CD spectrum of the **$Ag_{22}Cu_7$** cluster reminds of short-range oscillations that are added on top of a long-range envelope function and is therefore lacking from strongly characteristic pronounced features. Advantageous in calculations is that the origin of the chirality in this rather complex system can be analyzed. Figure S23 shows the rotatory strength transition contribution map (RTCM) that reveals the most important positive and negative contributions to the rotatory strength of the selected spectral feature as decomposed to Kohn-Sham basis. The first remarkable finding is that the two longest wavelength peaks have relatively high absolute intensity, close to the strongest found above 400 nm. Closer look reveals that these peaks are created by transitions between P- and D-symmetric superatom states, which means that they inherit the structural distortions of the metal core and become chirally active in contrary to the case of ideal spherical system. Spectral features between 400 nm and 700 nm are on average of lower intensity than the first two peaks. This may be caused because of the gap from the superatom states to the denser bands of the ligand states or because the chirality at the ligand layer is not as important as in the metal core. When going to shorter wavelengths below 400 nm, there starts to be considerably stronger peaks in the spectrum that are highly collective by nature. The main contributions can be depicted to come from various transitions from occupied ligand states between -3.0 eV and –1.5 eV to unoccupied ligand states between 1.5 eV and 3.0

eV. These states are localized in both alkynyls and phosphines as stated before and is shown in Figure S14.

Conclusion

In conclusion, we report the synthesis and total structure of $[Ag_{22}Cu_7(C{\equiv}CR)_{16}(PPh_3)_5Cl_6](PPh_4)$, an alkynyl-protected chiral bimetallic AgCu nanocluster with eight free valence electrons. It consists of an interpenetrating biicosahedral $Ag_{17}Cu_2$ core with a prolate shape protected by a long $Ag_5Cu_4(C{\equiv}CR)_{10}(PPh_3)_5Cl_4$ helix along with the $Cu(C{\equiv}CR)_2$, -C≡CR and Cl motifs. This nanocluster is found to be chiral with respect to its core, metal-ligand interface and the ligand layer, demonstrating multiple origins of chirality in a single nanoscale system. A pair of phosphine-moiety-containing chiral monoamine molecules is employed as optical enrichment agents, and the conversion of **$Ag_{22}Cu_7$** to corresponding enantiomers is successfully achieved. The DFT calculations well-reproduced the experimental optical spectral features of **$Ag_{22}Cu_7$** cluster and explained their origins. The superatom P- and D- states are the most important for the optical and the CD activity of the cluster. The role of the metal core to the chirality is vital as the ligand and ligand-metal interface states do not strengthen the CD-signal except at very high energies. Our chiral molecules-based strategy for the enrichment of enantiomeric nanoclusters from the racemic nanoclusters is anticipated to enable the optical enrichment of other metal nanoclusters. Furthermore, the obtained insights into the multiple origins of chirality through the atomic-level structure of nanoclusters may motivate further research on the chirality and its applications at distinct atomic-levels of diverse alloy nanoclusters.

Acknowledgements

T.H. acknowledges the financial support by the Research Center Program of the IBS (IBS-R006-D1) in Korea. M.S.B. acknowledges the IBS for the Young Scientist Fellowship (IBS-R006-Y2). N.F.Z. thanks the National Key R&D Program of China (2017YFA0207302) and the NNSF of China (21890752, 21731005, 21721001) for financial support. The computational work at University of Jyväskylä was supported by the Academy of Finland (grants 292352, 294217, and 319208). The computations were performed at the Finnish national supercomputing center CSC.

Conflict of interest

The authors declare no competing financial interest.

Keywords: chirality • chirality origins • bimetallic cluster • superatom • alkynyl ligand

[1] a) X. Kang, Y. W. Li, M. Z. Zhu, R. C. Jin, *Chem. Soc. Rev.* **2020**, *49*, 6443-6514; b) R. C. Jin, C. J. Zeng, M. Zhou, Y. X. Chen, *Chem. Rev.* **2016**, *116*, 10346-10413; c) I. Chakraborty, T. Pradeep, *Chem. Rev.* **2017**, *117*, 8208-8271; d) K. Y. Zheng, J. P. Xie, *ACS Nano* **2020**, *14*, 11533-11541.

[2] a) Z. Lei, X. K. Wan, S. F. Yuan, Z. J. Guan, Q. M. Wang, *Acc. Chem. Res.* **2018**, *51*, 2465-2474; b) M. M. Zhang, X. Y. Dong, Y. J. Wang, S. Q. Zang, T. C. W. Mak, *Coord. Chem. Rev.* **2022**, *453*, 214315.

[3] a) P. D. Jadzinsky, G. Calero, C. J. Ackerson, D. A. Bushnell, R. D. Kornberg, *Science* **2007**, *318*, 430-433; b) A. Desireddy, B. E. Conn, J. S. Guo, B. Yoon, R. N. Barnett, B. M. Monahan, K. Kirschbaum, W. P. Griffith, R. L. Whetten, U. Landman, T. P. Bigioni, *Nature* **2013**, *501*, 399-402.

[4] a) M. M. Zhang, X. Y. Dong, Z. Y. Wang, X. M. Luo, J. H. Huang, S. Q. Zang, T. C. W. Mak, *J. Am. Chem. Soc.* **2021**, *143*, 6048-6053; b) M. M. Zhang, X. Y. Dong, Z. Y. Wang, H. Y. Li, S. J. Li, X. L. Zhao, S. Q. Zang, *Angew. Chem. Int. Ed.* **2020**, *59*, 10052-10058; c) F. Hu, Z. J. Guan, G. Y. Yang, J. Q. Wang, J. J. Li, S. F. Yuan, G. J. Liang, Q. M. Wang, *J. Am. Chem. Soc.* **2021**, *143*, 17059-17067; d) Q. Y. Wang, J. Wang, S. Wang, Z. Y. Wang, M. Cao, C. L. He, J. Q. Yang, S. Q. Zang, T. C. W. Mak, *J. Am. Chem. Soc.* **2020**, *142*, 12010-12014.

[5] a) Z. J. Guan, J. L. Zeng, S. F. Yuan, F. Hu, Y. M. Lin, Q. M. Wang, *Angew. Chem. Int. Ed.* **2018**, *57*, 5703-5707; b) Y. Wang, H. F. Su, C. F. Xu, G. Li, L. Gell, S. C. Lin, Z. C. Tang, H. Häkkinen, N. F. Zheng, *J. Am. Chem. Soc.* **2015**, *137*, 4324-4327; c) Y. Wang, X. K. Wan, L. T. Ren, H. F. Su, G. Li, S. Malola, S. C. Lin, Z. C. Tang, H. Häkkinen, B. K. Teo, Q. M. Wang, N. F. Zheng, *J. Am. Chem. Soc.* **2016**, *138*, 3278-3281; d) P. Yuan, R. H. Zhang, E. Selenius, P. P. Ruan, Y. R. Yao, Y. Zhou, S. Malola, H. Häkkinen, B. K. Teo, Y. Cao, N. F. Zheng, *Nat. Commun.* **2020**, *11*, 2229; e) X. T. Yuan, S. Malola, G. C. Deng, F. J. Chen, H. Häkkinen, B. K. Teo, L. S. Zheng, N. F. Zheng, *Inorg. Chem.* **2021**, *60*, 3529-3533; f) J. L. Zeng, Z. J. Guan, Y. Du, Z. A. Nan, Y. M. Lin, Q. M. Wang, *J. Am. Chem. Soc.* **2016**, *138*, 7848-7851.

[6] X. K. Wan, X. L. Cheng, Q. Tang, Y. Z. Han, G. X. Hu, D. E. Jiang, Q. M. Wang, *J. Am. Chem. Soc.* **2017**, *139*, 9451-9454.

[7] S. C. K. Hau, M. C. L. Yeung, V. W. W. Yam, T. C. W. Mak, *J. Am. Chem. Soc.* **2016**, *138*, 13732-13739.

[8] T. U. Connell, S. Sandanayake, G. N. Khairallah, J. M. White, R. A. J. O'Hair, P. S. Donnelly, S. J. Williams, *Dalton Trans.* **2013**, *42*, 4903-4907.

[9] Z. H. Chen, L. Y. Zhang, Z. N. Chen, *Organometallics* **2012**, *31*, 256-260.

[10] H. Shen, Y. Z. Han, Q. Y. Wu, J. Peng, B. K. Teo, N. F. Zheng, *Small Methods* **2020**, *5*, 2000603.

[11] X. S. Ma, L. Xiong, L. B. Qin, Y. Tang, G. Y. Ma, Y. Pei, Z. H. Tang, *Chem. Sci.* **2021**, *12*, 12819-12826.

[12] a) M. Z. Zhu, H. F. Qian, X. M. Meng, S. S. Jin, Z. K. Wu, R. C. Jina, *Nano Lett.* **2011**, *11*, 3963-3969; b) C. J. Zeng, R. C. Jin, *Chem. Asian J.* **2017**, *12*, 1839-1850; c) C. Gautier, T. Bürgi, *J. Am. Chem. Soc.* **2008**, *130*, 7077-7084; d) C. Gautier, T. Burgi, *J. Am. Chem. Soc.* **2006**, *128*, 11079-11087; e) G. C. Deng, S. Malola, J. Z. Yan, Y. Z. Han, P. Yuan, C. W. Zhao, X. T. Yuan, S. C. Lin, Z. C. Tang, B. K. Teo, H. Häkkinen, N. F. Zheng, *Angew. Chem. Int. Ed.* **2018**, *57*, 3421-3425. f) O. Lopez-Acevedo, H. Tsunoyama, T. Tsukuda, H. Häkkinen, C. M. Aikens, *J. Am. Chem. Soc.* **2010**, *132*, 8210-8218.

[13] a) C. J. Zeng, Y. X. Chen, K. Kirschbaum, K. Appavoo, M. Y. Sfeir, R. C. Jin, *Sci. Adv.* **2015**, *1*, e1500045; b) W. D. Si, Y. Z. Li, S. S. Zhang, S. N. Wang, L. Feng, Z. Y. Gao, C. H. Tung, D. Sun, *ACS Nano* **2021**, *15*, 16019-16029; c) L. Liao, S. Zhuang, C. Yao, N. Yan, J. Chen, C. Wang, N. Xia, X. Liu, M.-B. Li, L. Li, X. Bao, Z. Wu, *J. Am. Chem. Soc.* **2016**, *138*, 10425-10428; d) X. Q. Liang, Y. Z. Li, Z. Wang, S. S. Zhang, Y. C. Liu, Z. Z. Cao, L. Feng, Z. Y. Gao, Q. W. Xue, C. H. Tung, D. Sun, *Nat. Commun.* **2021**, *12*, 4966; e) Y. N. Wang, B. Nieto-Ortega, T. Bürgi, *Nat. Commun.* **2020**, *11*, 4562; f) I. Dolamic, S. Knoppe, A. Dass, T. Burgi, *Nat. Commun.* **2012**, *3*, 798; g) R. W. Y. Man, H. Yi, S. Malola, S. Takano, T. Tsukuda, H. Häkkinen, M. Nambo, C. M. Crudden, *J. Am. Chem. Soc.* **2022**, *144*, 2056-2061; h) S. Ito, S. Takano, T. Tsukuda, *J. Phys. Chem. Lett.* **2019**, *10*, 6892-6896; i) G. C. Deng, S. Malola, P. Yuan, X. H. Liu, B. K. Teo, H. Häkkinen, N. F. Zheng, *Angew. Chem. Int. Ed.* **2021**, *60*, 12897-12903; j) M. S. Bootharaju, H. Chang, G. C. Deng, S. Malola, W. Baek, H. Hakkinen, N. F. Zheng, T. Hyeon, *J. Am. Chem. Soc.* **2019**, *141*, 8422-8425.

[14] Deposition Number 2171994 contains the supplementary crystallographic data for this paper. These data are provided free of charge by the joint Cambridge Crystallographic Data Centre and Fachinformationszentrum Karlsruhe Access Structures service www.ccdc.cam.ac.uk/structures.

[15] a) M. S. Bootharaju, S. M. Kozlov, Z. Cao, M. Harb, N. Maity, A. Shkurenko, M. R. Parida, M. N. Hedhili, M. Eddaoudi, O. F. Mohammed, O. M. Bakr, L. Cavallo, J. M. Basset, *J. Am. Chem. Soc.* **2017**, *139*, 1053-1056; b) T. U. B. Rao, B. Nataraju, T. Pradeep, *J. Am. Chem. Soc.* **2010**, *132*, 16304-16307; c) W. T. Chang, S. Sharma, J. H. Liao, S. Kahlal, Y. C. Liu, M. H. Chiang, J. Y. Saillard, C. W. Liu, *Chem. Eur. J.* **2018**, *24*, 14352-14357.

[16] a) X. K. Wan, W. W. Xu, S. F. Yuan, Y. Gao, X. C. Zeng, Q. M. Wang, *Angew. Chem. Int. Ed.* **2015**, *54*, 9683-9686; b) M. Qu, H. Li, L. H. Xie, S. T. Yan, J. R. Li, J. H. Wang, C. Y. Wei, Y. W. Wu, X. M. Zhang, *J. Am. Chem. Soc.* **2017**, *139*, 12346-12349.

[17] J. Enkovaara, C. Rostgaard, J. J. Mortensen, J. Chen, M. Dułak, L. Ferrighi, J. Gavnholt, C. Glinsvad, V. Haikola, H. A. Hansen, H. H. Kristoffersen, M. Kuisma, A. H. Larsen, L. Lehtovaara, M. Ljungberg, O.

Lopez-Acevedo, P. G. Moses, J. Ojanen, T. Olsen, V. Petzold, N. A. Romero, J. Stausholm-Møller, M. Strange, G. A. Tritsaris, M. Vanin, M. Walter, B. Hammer, H. Häkkinen, G. K. H. Madsen, R. M. Nieminen, J. K. Nørskov, M. Puska, T. T. Rantala, J. Schiøtz, K. S. Thygesen, K. W. Jacobsen, *J. Phys.: Condens. Matter* **2010**, *22*, 253202.

[18] J. Z. Yan, H. F. Su, H. Y. Yang, C.Y. Hu, S. Malola, S. C. Lin, B. K. Teo, H. Häkkinen, N. F. Zheng, *J. Am. Chem. Soc.* **2016**, *138*,12751–12754.

[19] J. H. Huang, Y. B. Si, X. Y. Dong, Z. Y. Wang, L. Y. Liu, S. Q. Zang, T. C. W. Mak, *J. Am. Chem. Soc.* **2021**, *143*, 12439-12444.

[20] a) S. Knoppe, I. Dolamic, T. Bürgi, *J. Am. Chem. Soc.* **2012,** *134*, 13114-13120; b) N. Barrabés, B. Zhang, T. Bürgi, *J. Am. Chem. Soc.* **2014**, *136*, 14361-14364.

[21] S. Malola, H. Häkkinen, *Chem. Commun.* **2019**, *55*, 9460-9462.

10.1002/anie.202217483

Entry for the Table of Contents

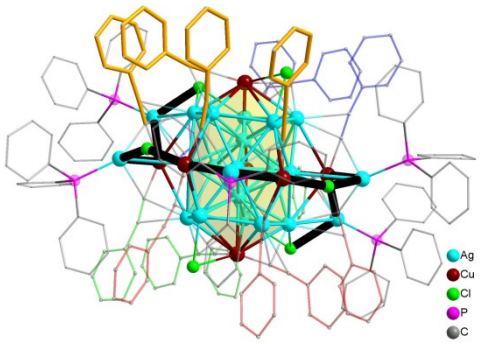

An alkynyl-protected chiral bimetallic AgCu superatomic nanocluster $[Ag_{22}Cu_7(C{\equiv}CR)_{16}(PPh_3)_5Cl_6]^-$ with a high free valence electron count is reported. This cluster exhibits multiple chirality origins, including the metal core, metal-ligand interface and ligand layer.